Peer-reviewed version available at Aerospace 2019, 6, 16; doi:10.3390/aerospace6020016

Article

Conjugate heat transfer characteristics in a highly thermally loaded film cooling configuration with TBC in syngas

Jing Ren[1,*], Xueying Li [1,†] and Hongde Jiang [1,†]

[1] Institute of Gas Turbine, Department of Energy and Power Engineering, Tsinghua University; renj@tsinghua.edu.cn
* Correspondence: ren@tsinghua.edu.cn; Tel.: +86-10-62796401
† These authors contributed equally to this work.

Abstract: The future power equipment tends to take hydrogen or middle/low heat-value syngas as fuel for low emission. The heat transfer of film cooled turbine blade shall be influenced more by radiation. Its characteristic of conjugate heat transfer is studied experimentally and numerically in the paper by considering radiation heat transfer, multi-composition gas and TBC. The Weighted Sum of Gray Gases spectral model and Discrete Transfer Model are utilized to solve the radiative heat transfer in the multi-composition field, while validated against the experimental data for the studied cases. It is shown that the plate temperature increases significantly when considering the radiation and the temperature gradient of the film cooled plate becomes larger. It is also shown that increasing percentage of steam in gas composition results in increased temperature on the film-cooled plate. The normalized temperature of the film-cooled plate decreases about 0.02, as the total percentage of steam in hot gas increases per 7%. As for the TBC effect, it can smooth out the the temperature distribution and insulate the heat to a greater extent when the radiative heat transfer becomes significant.

Keywords: film cooling; conjugate heat transfer; radiation; syngas; TBC

1. Introduction

The future advanced power generation cycles are supposed to utilize hydrogen or middle/low heat-value syngas as fuel, aiming to realize Zero-Emission or Near-Zero Emission. In detail, the thermal performance of turbines depends on moist gases composition. Furthermore, the radiative heat transfer can be enhanced when the turbine inlet temperature grows. Also, the varied gas composition due to fuel variation will impact the turbine heat transfer performance, since steam and carbon dioxide are far more radiative than air or nitrogen diluted gas stream [1]. The thermal barrier coating (TBC), as a semitransparent medium for radiation, is influenced by the gas compositions and radiation at the same time. Therefore, it is important to predict temperature distribution of thermal components accurately, especially considering radiative heat transfer.

The conjugate heat transfer method is widely adopted in the design of the high-thermal loaded components of gas turbines. Bohn et al. [2-7] used the self-developed code and conducted comprehensive studies on the conjugate heat transfer performance of turbomachinery. Mansour et al. [8] investigated the effect of transition model on the accuracy of conjugate heat transfer simulation. Heidmann [9] investigated the boundary element method (BEM) in simulating the three-dimensional film-cooled turbine vane, and two materials with different thermal conductivity were considered. The work of Hylton et al. [10-11] conducted detailed surface temperature measurements at the

midspan of the Mark II and the C3X vanes. The data of Hylton is widely used as benchmark date for conjugate heat transfer simulations. Recently, Dees and Bogard et al. [12-14] conducted a series of experiments of a turbine vane including adiabatic and conjugate heat transfer conditions.

Efforts focused on the effects of radiative heat transfer on the gas turbine have been widely conducted. Kumar and Kale [15] conducted conjugate heat transfer simulation of a two-dimensional blade by a FEM based numerical scheme. The computational results showed that the radiative heat transfer was decreased if the TBC was included. He and Tan [16] simulated the radiatice heat transfer process in a three-dimensional engine vane adopting the discrete ordinates model. The results indicated that the incident radiative heat fluxes increase from 188% to 212% as the inlet gas temperature increase 29.9%. Zhang et al. [17] utilized a coupled fluid-thermal model to investigate the conjugate heat transfer characteristics of 3D turbine blade by adopting P-1 radiation model. It was shown that the blade surface temperature increased significantly and varied a lot when considering the inlet radiation. Akwaboa et al. [18] investigated the combined effects of radiation heat transfer and heat conduction in the semitransparent TBCs. Their results showed that the temperature of the metal substrate with TBC exceeded over about 40 K than that without radiation. Mazzotta et al. [19] investigated the temperature distribution on a E3 airfoil with the turbine inlet temperature exceeding 1700°C. They considered varied gas compositions, with employing P-1 model for solving radiative heat transfer equation. It was shown that the contribution of radiation on the total surface heat flux was up to 5.7%.

The effect of the hot gas compositions on the turbine heat transfer performance was also investigated in recent studies. S. Na et al. [20] studied the effect of varying hot gas composition on the temperature distribution of flat plate. The results showed that varying hot gas composition has a significant influence on the maximum temperature distribution of a film-cooled flat plate. Moliere et.al [21] reported that increasing 1% radiative heat transfer resulted in a temperature increment of 2.3K on the airfoil surface. As for the TBC, Feuerstein [22] reviewed the effect of TBC materials on the thermal performance of turbine airfoil. Bohn et al. and Davidson et al. [23, 24] investigated the effect of TBC on the temperature distribution of gas turbine.

In the present study, a high temperature test rig was built up to investigate the conjugate heat transfer performance of a flat plate with a row of film cooling holes, considering the combination of conduction, convection and radiation. The hot gas is about 800°C while the coolant air about 400°C. The present study reviews the thermal performance considering the radiation heat transfer, hot gas composition, and TBC. The hot gas compositions are the combustion products of liquefied petroleum gas (LPG), natural gas (NG), syngas (syn), hydrogen (H_2) and oxy-fuel gas (oxy). Both experimental and numerical methods are employed to understand the interaction among conjugate heat transfer, gas compositions and TBC.

2. Experimental Apparatus

Figure 1 shows the highly thermal-loaded film cooling test rig, which is built up in Tsinghua University, China. The test rig is composed of five main parts: the hot main gas inlet system, the coolant air supply system, the film plate test section, the exhaust section and the measurement system. The five parts will be described in detail in the following sections.

Figure 1. Highly thermally loaded film cooling test rig

2.1. Hot Gas And Coolant Air Supply Systems

Figure 2 shows the schematic representation of the test rig. The hot main gas system includes fuel injection section and burner section and produce hot gas with temperature of 800 °C. The fuel is mixed with air and is ignited in a 380Mcal/h burner. The fuel is liquefied Petroleum Gas (LPG) and has a flow rate from 15 to 30 kg/h, regulating the burner output power at a range of 200~400Mcal/h. The combustion products leave the burner with a temperature of about 2000 °C and entered the diluting section. The hot gas is mixed with the diluting air and the sprayed water, supplied by the top blower and the water supply system respectively. The resulting hot multi-composition gas is 800 °C.

The second system is the water supply system, which is used to adjust the hot gas composition with water. Eight spraying nozzles are spaced equally around the diluting section, delivering the diluting water into the section. The water flow rate is adjusted by the water supply pressure. The secondary coolant air is generated by a second blower and then is heated by an electric heat exchanger. The resulting air temperature is about 400 °C. Both the mainstream and coolant air channels are covered with heat-insulated layers.

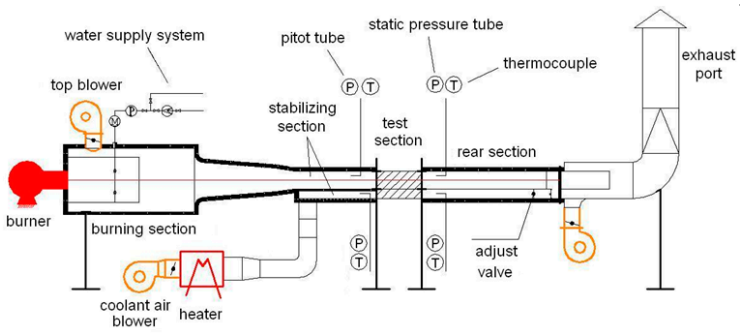

Figure 2. Schematic representation of test rig

2.2. Test Section

The test section is composed of internal cooling side and film cooling side, which is a typical cooling section of a turbine airfoil. The film cooling side hot gas temperature is 800 °C and the internal cooling side air temperature is 400 °C. The film cooling side and the internal cooling side are separated by a nickel-based superalloy flat plate with a thickness of 18 mm, as shown in Fig. 3. A row of seven film holes are arranged on the nickel-based superalloy plate, with a hole diameter of 8 mm. The film hole pitch is 3D, the hole inclination angle is 35°, and the length of the hole is L=3.92 D. The distance between the trailing edge of the holes and the inlet of the plate is 11D, while between the trailing edge of the holes and the outlet of the plate is 42D. On the top surface of the superalloy plate, TBC is sprayed by utilizing APS (Air Plasma Spraying) method, which is shown in Fig. 4. The top

Preprints (www.preprints.org) | NOT PEER-REVIEWED | Posted: 15 November 2018 doi:10.20944/preprints201811.0343.v1

Peer-reviewed version available at Aerospace 2019, 6, 16; doi:10.3390/aerospace6020016

coat is 0.5mm thick and the bond coat is 0.2mm thick. The thermal conductivities of the superalloy plate and TBC are 20W/mK and 2W/mK, respectively. But they will change with temperature.

The hot gas and the coolant air are at a speed of 15~20 m/s. An adjustable valve is installed in the cooling air channel, and by decreasing the flow area of the coolant air channel, the back pressure of the coolant air channel is higher than that of the hot gas channel. The blowing ratios are varied by adjusting the coolant and mainstream pressure difference.

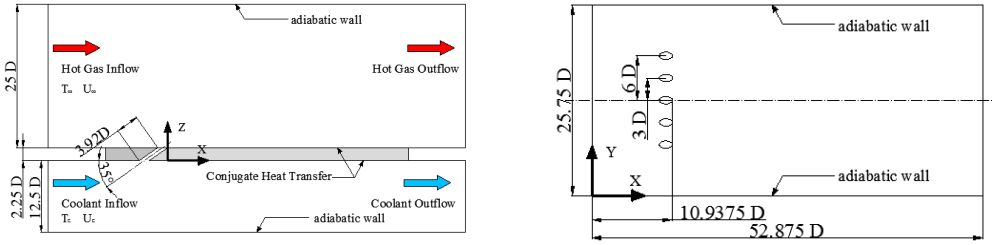

Figure 3. Schematic drawing of the test section, (**a**) Front view of the test section; (**b**) Top view of the film cooled plate

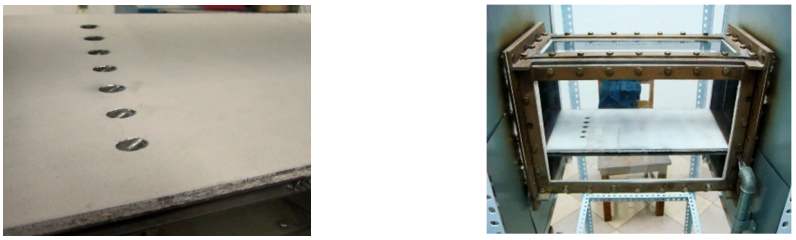

Figure 4. Superalloy plate and test section, (**a**) Photo of the superalloy plate; (**b**) Photo of the test section

2.3. Measurement System

The measuring system includes the pitot tubes, the static pressure tubes, the thermocouples, and the chromatographic analyzer. Four thermocouple are implemented at the center point of inlet and outlet of mainstream channel and coolant channel, measuring the temperatures of the inflow and the outflow, as shown in Fig.2. The inflow velocity is obtained by two pitot tubes that are installed in the center of each channel at the inlet of the test section. The back pressures of the channels are acquired by the static pressure tubes located at the outlet of the test section. In the downstream area of the centered film cooling hole, 90 thermocouples are installed on both top surface, bottom surface and middle of the plate, as shown in Fig. 5 and Table 1. The gas collecting tube locates at the stabilizing section of the hot main gas channel. The composition of the hot gas is determined by the chromatographic analyzer from the gas sample collected.

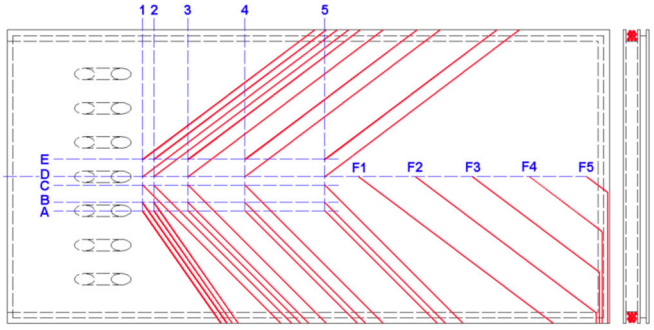

Figure5. Schematic drawing of thermos couple positions on the plate

Table 1. Positions of the thermocouples.

Thermal couple positions	1	2	3	4	5	F1	F2	F3	F4	F5
Distance from the trailing edge of the hole to the thermocouple	1 D	2 D	5 D	10 D	17 D	20 D	25 D	30 D	35 D	40 D

The measurement uncertainty of the thermocouple is 0.3% and of chromatographic analyzer is 2.2%. The uncertainty of the test system for temperature measurement is about 2.3%. The correction factors of the pitot tubes and the static tubes are calibrated to be unity.

3. Numerical Methodology

The numerical algorithm applied in the present study is conjugate heat transfer method, which consider the thermal conduction, convection and radiation in the computation. Commercial software ANSYS CFX 12.1 is adopted for all the numerical studies. The radiation heat transfer equation is solved by utilizing the discrete transfer radiation model (DTM). The absorption coefficient of the gas is determined by the weighted sum of gray gases (WSGG) spectral model. The numerical method is validated by comparing computational results with the experimental data.

3.1. Test Section Radiation Model

In the present study, the discrete transfer model (DTM) is employed due to the optical thickness of the radiation is less than unity. The DTM depends upon the discretization of the equation of transfer along multiple rays leaving from the bounding surfaces. The radiation transport governing equation is expressed as follows:

$$\frac{dI_v\left(\vec{r},\vec{s}\right)}{ds}=-\left(K_{av}+K_{sv}\right)I_v\left(\vec{r},\vec{s}\right)+K_{av}I_{bv}\left(v,T\right)+\frac{K_{sv}}{4\pi}\int_{4\pi}I_v\left(\vec{r},\vec{s}'\right)d\Omega'+S \quad (1)$$

The DTM is based on the assumption that operating system is homogeneous. the intensity *Iv* is solved along the rays leaving from the boundaries in the following form:

$$I_v\left(\vec{r},\vec{s}\right)=I_{vo}\exp\left(-\left(K_{av}+K_{sv}\right)s\right)+I_{bv}\left(1-\exp\left(-K_{av}s\right)\right)+K_{sv}\overline{I_v} \quad (2)$$

The homogeneity assumption is maintained to extend the solution to the entire domain. It is then integrated over a solid angle to obtain the spectral incident radiation and the radiative heat flux at discrete points.

3.2. Spectral Model

For computation of the gas radiation properties, the weighted sum of gray gases (WSGG) model is the most widely model option, which is a compromise between the complete model that considers the particular absorption bands [25] and the oversimplified gray gas model. The WSGG model is combined with the DTM to obtain the emissivity of H_2O and CO_2. In the WSGG model, the gas emissivity is a weighted sum of gray gas emissivity in the following expression:

$$\varepsilon=\sum_{j=0}^{N_g}a_j\left(T\right)\left[1-\exp\left(k_j s\right)\right] \quad (3)$$

where a_j and k_j are the weighting factor and the absorption coefficient for the j_{th} gray gas component, respectively. The s is the path length. There exists a constraint that the sum of coefficients a_j is equal to unity when calculating coefficients of a_j and k_j. The transparent regions of the spectrum are

indicated by the term $j = 0$. The coefficients (a_j and k_j) from references [26] and [27] are used in the study. The partial pressure ratios of H_2O and CO_2 (H_2O/CO_2) are 1 and 2 when the number of gray gases is 3 [26]. The coefficients are applied when gas temperature falls within the range of 600 to 2000 K and the partial pressure-path length products are from 0.001 to 10.0 atm-m. The property values are adequately predicted and are designated as "Smith 4GG". The partial pressure ratios of H_2O and CO_2 (H_2O/CO_2) are 2 and 3 when the number of gray gases is 4 [27]. The model is designated as "Perry 5GG". A more detailed description of the model can be found in reference [28].

3.3. Computational Geometry and Domain

The computational geometry is similar to the test section, including hole geometries, coolant and mainstream supply system. The inlet and outlet sections are extended by 10D to generate stable flow boundary conditions as shown in Fig. 6. Figure 7 shows the multi-block structured mesh, which is refined near the film-cooling holes and near-wall regions. More than 10 points are implemented in the boundary layer to achieve y+ less than unity. The total element amount of the mesh is about 7.94 million. A grid refinement is conducted to generate a mesh with 12.20 million cells and check mesh independent study. The results show that the two sets of meshes behave quite similar, and hence the mesh with 7.94 million cells is adopted in the present simulations.

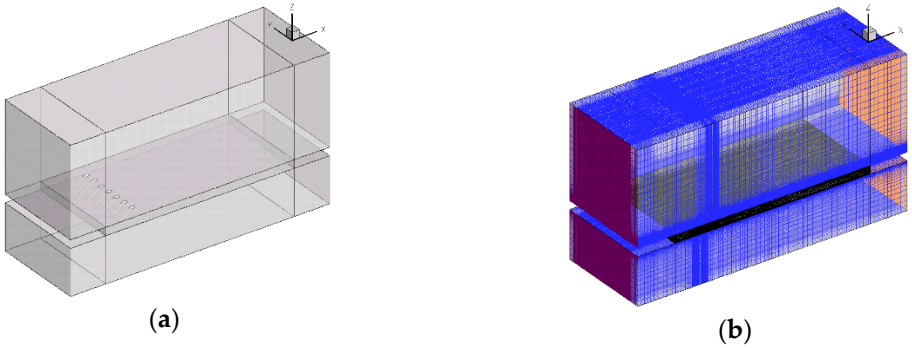

(**a**) (**b**)

Figure6. Computational domain and the structured mesh (**a**) Computational domain; (**b**) Multi-block structured mesh.

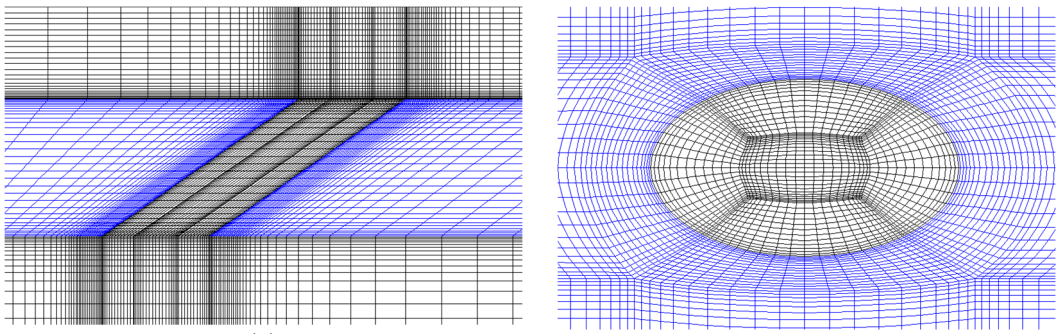

(**a**) (**b**)

Figure7. Details of the structured mesh, (**a**) refined mesh near the plate; (**b**) refined mesh around the film cooling hole.

3.4. Turbulence model and Boundary Conditions

The SST *k-ω* turbulence model of Menter is adopted in the steady RANS simulations. The k-ω model is used in near wall regions and the *k-ε* model is switched on in mainstream region. The mass flow rate boundary condition is applied at the inlet section and steady pressure is applied at the outlet section. The top and bottom surfaces of the test plate are heat transfer interface between fluid and solid domain. The other walls around the fluid domain are temperature wall, and the temperatures are measured by thermocouples.

3.5. Material Parameters

In the present simulations, the specific heat and thermal conductivity of the nickel-based superalloy vary with temperature and are provided in reference [29]. The emissivity of the Nickel-based superalloy plate is set as 0.79 [30]. Ideal gas assumption is used in the simulations, where the specific heat capacity of the gas is calculated by the NASA format polynomials. The gas transport properties are obtained from the REFPROP program that is an acronym for reference fluid properties [31].

3.6. Validation of the numerical algorithm

Based on the configuration of the test rig, three gas composition cases are studied to validate the numerical algorithm. The gas compositions of each case are listed in Table 2. Varying the steam humidity of hot gas can change the gas composition. Other boundary conditions of the three experimental cases keep the constant, which is shown in Table 3.

Table 2. The experimental hot gas compositions

Compositions (Volume %)	Case 1	Case 2	Case 3
H_2O	11.86	22.34	26.15
CO_2	5.28	7.14	7.80
O_2	10.26	5.55	3.87
N_2	72.60	64.97	62.18

Table 3. Experimental boundary conditions

Parameters	Mainstream	Coolant Flow
Inlet Temperature[℃]	800	389
Inlet Mass Flow Rate [kg/s]	0.217	0.140
Outlet Pressure [pa]	101407	101428

Figure 8 shows the experimental and numerical centerline temperature distribution along the centerline on the top and bottom plate surfaces. The red line indicates temperature distribution on the top surface, and the green line indicates the temperature distribution on the bottom surface. It is shown that the numerical results agree well with the experimental results for three cases. Therefore, it is concluded that the DTM and WSGG model are adequately accurate for the present cases.

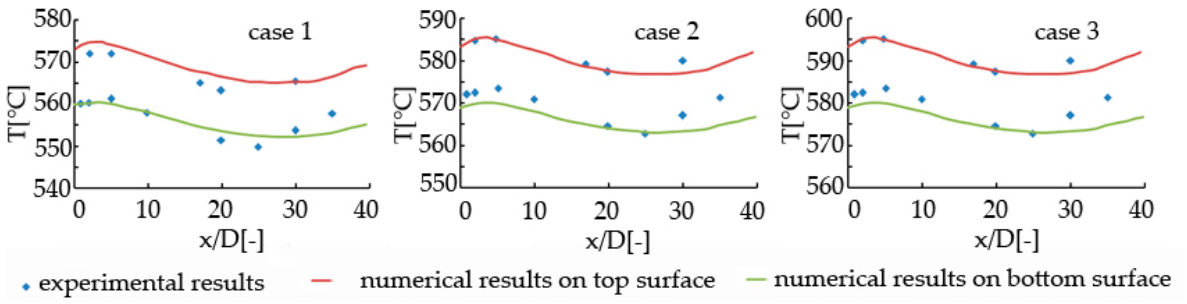

Figure8. Centerline temperature distribution on the top and bottom surfaces of the film cooled plate

4. Results and Discussion

4.1. Effect of Radiative Heat Transfer

A pair of numerical cases with/without radiation are carried on to study the effect of radiative heat transfer based on the validated algorithm. The numerical study corresponds to a selected test cases with a mass fraction of H_2O is 7.92. The detailed information of the selected test case could be found in the Ref. 32.

The temperature distributions on the top and bottom sides of film plate resulted from the numerical study are showed in Fig. 9 for both with/without radiation cases. It is noted that the temperature level is significantly increased after considering the radiation for both the upper and bottom surfaces. Also the temperature patterns are changed if the plate is subjected to radiation, especially on the top surface where film cooling occurs.

Continually, the spanwise averaged temperature profiles on the top plate surface in both cases are shown in Fig. 10. It is noted that, on both top and bottom surfaces near the film cooling hole, the temperature profile in the spanwise direction becomes smoother when considering the radiation. This means radiation decreases the temperature gradient in the spanwise direction.

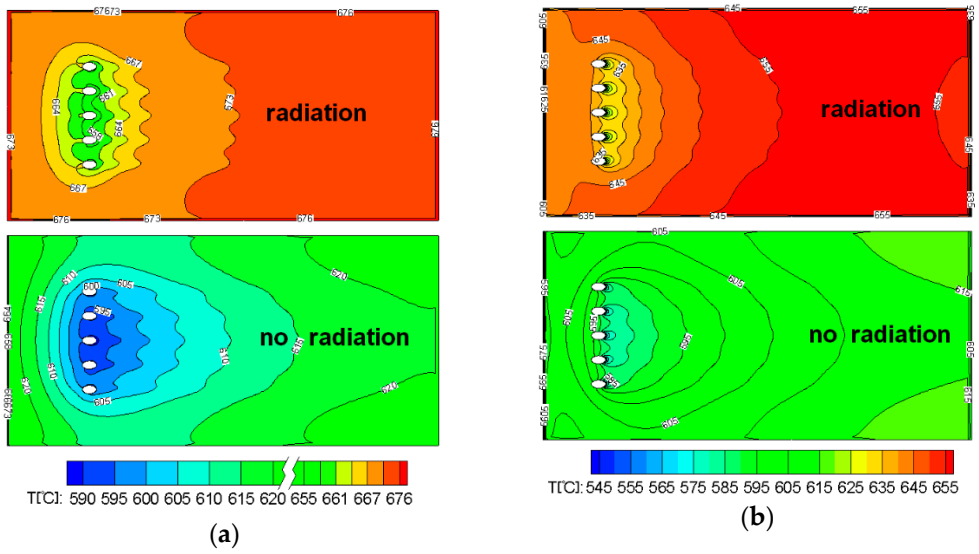

Figure9. Temperature distribution with/without radiation (**a**) on the top surface; (**b**) on the bottom surface.

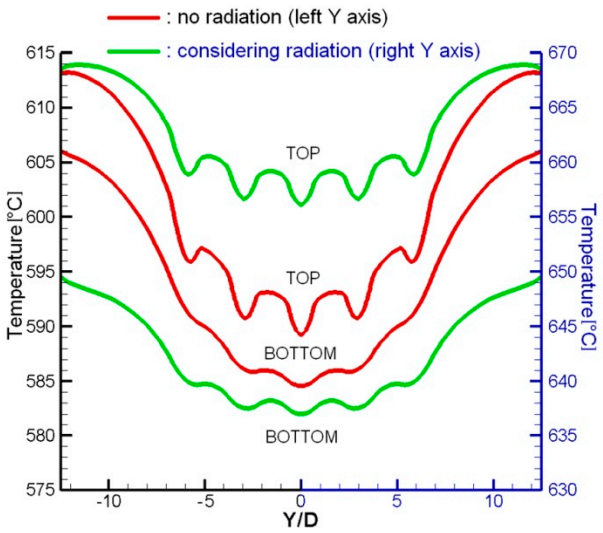

Figure10. Spanwise averaged temperature profile on the top plate surface, X/D=1

To further quantify the effect of radiative heat transfer, a normalized temperature η is defined by the following expression:

$$\eta = \frac{(T_w - T_c)}{T_g - T_c} \tag{4}$$

where *Tg*, *Tc*, *Tw* are the temperatures of the hot gas, the coolant air and the top surface wall. The normalized temperature is similar to the film cooling effectiveness when the plate surface is adiabatic.

Figure 11 shows line plots of η along the centerline of the plate top surface, an adiabatic case is employed as the basic. Compares with the case with no radiation, the normalized temperature of the case with radiation is about 0.2 lower, and even is lower than the adiabatic effectiveness before x = 13D, the high cooling effectiveness near the holes almost disappears. That is to say, the film cooling effect is weakened by radiation while it further smears out the temperature gradient. In real engine conditions, hot main gas temperature will be higher than 1200℃ (much higher than the condition of the test rig), and leads to high surface temperature and high local temperature gradient, which will result in significant thermal-mechanical load. The radiation enhances the temperature increasing, but weakens the temperature gradient.

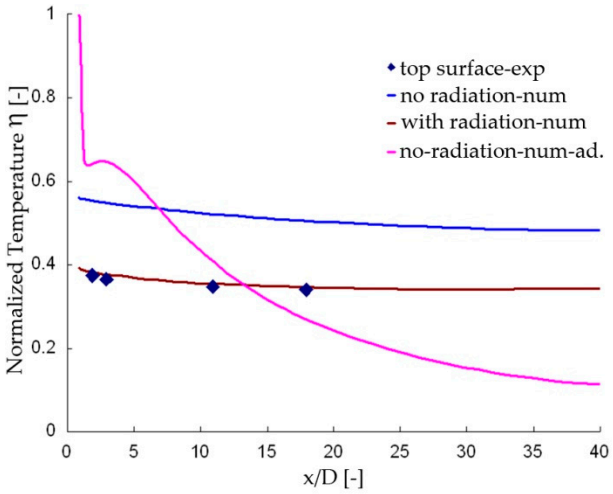

Figure11. Normalized temperature along the centerline of the top plate surface

4.2. Effect of Hot Gas Composition

The effect of the hot gas composition on the film cooling system is investigated by varying five different kinds of fuel. The hot gas compositions for each fuel are listed in Tab. 4.

Table 4. Hot gas compositions in the numerical study[1]

Type of Fuel	Mole fraction [%]				
	CO_2	H_2O	N_2	Ar	O_2
LPG	4.44	12.34	71.50	0.00	11.72
NG	5.66	11.08	74.66	0.00	8.60
Syn	9.27	8.50	72.80	0.80	8.63
H_2	1.40	17.30	72.20	0.90	8.20
Oxy	16.00	82.00	1.10	0.80	0.10

[1] The hot gas are the products of combustion of liquid petroleum gas (LPG), natural gas (NG), syngas (syn), hydrogen gas (H_2), and oxy-fuel gas (oxy).

Figure 12 shows the temperature distribution along the centerline of the top surface for five different fuels, with and without considering the radiation. Without considering radiative heat transfer, the temperature distributions are similar for five different fuel cases. Nitrogen is the major

composition of the hot gases and its mole fraction is more than 70%, while steam is the major composition of the combustion product of oxy and its mole fraction is 82%. Therefore, it is observed that the temperature distribution for the combustion product of oxy is about 15 °C higher than the other four gases. When considering the radiative heat transfer, a temperature rise about 50 °C is observed. A great temperature rise occurs for the combustion product of the natural gas has, which leads to a quite close temperature distribution to that of the combustion product of the oxy-fuel gas.

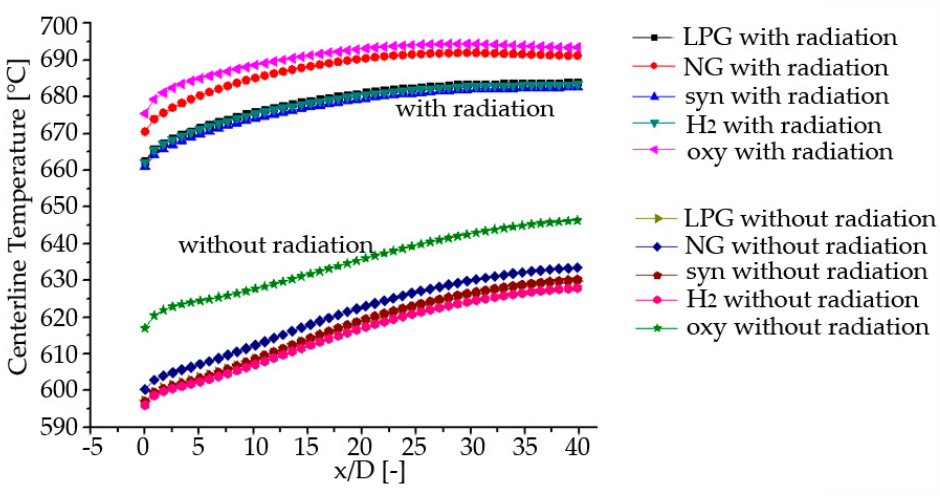

Figure12 Temperature distribution along the centerline of the plate with/without radiation

4.3. Effect of Thermal Barrier Coating (TBC)

The effect of thermal barrier coating on the heat transfer performance is experimentally investigated. three different hot gas compositions are investigated after spraying TBC on the top surface of the plate. Table 5 shows the different gas compositions with and without TBC.

Table 5. Hot gas compositions in experiments with/without TBC.

Compostions (Volume %)	Case 1 Without TBC	Case 1 With TBC	Case 2 Without TBC	Case 2 With TBC	Case 3 Without TBC	Case 3 With TBC
H_2O	11.86	11.27	22.34	22.66	26.15	25.01
CO_2	5.28	6.13	7.14	6.23	7.80	8.65
O_2	10.26	10.07	5.55	5.25	3.87	4.94
N_2	72.60	72.53	64.97	65.86	62.18	61.40

Figure 13 shows the experimental centerline temperature results on the top and bottom sides of the film plate. It is observed that the temperature patterns show a quite similar trend with and without TBC. In particular, the temperature is at high value the inlet, then decreases as x/D increases, and increases at the downstream region.

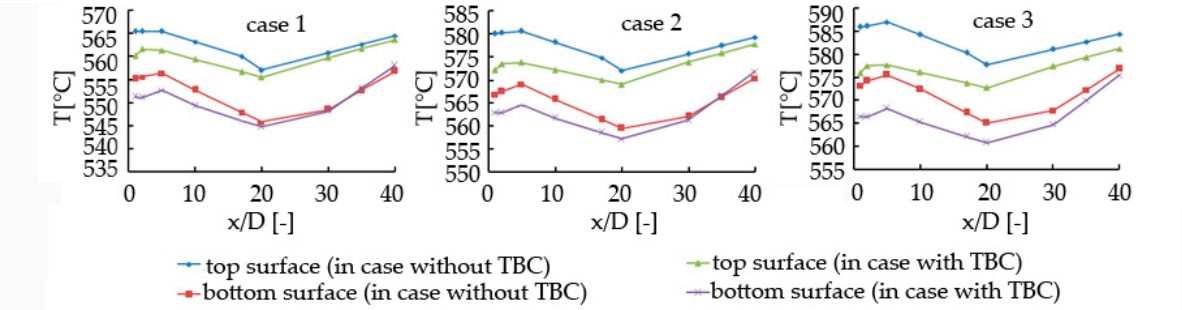

Figure13. Temperature along the centerline of the test plate surface

The temperature drops inside TBC are shown in Fig.14, which is derived from the results of three pair of cases. It is clear that, in case 3, a higher percentage of steam results in a greater temperature drop. By observing the temperature drop distribution with x/D, it is observed that the temperature drop reaches maximum value at the entrance section, and decrease as x/D increases. This is associated with the radiation distribution feature, i.e., a larger humidity causes a stronger radiation. Therefore, the radiation is strongest at the entrance section, and grows weaker as x/D increases, which indicates the temperature drop by TBC is higher when radiation effect is stronger.

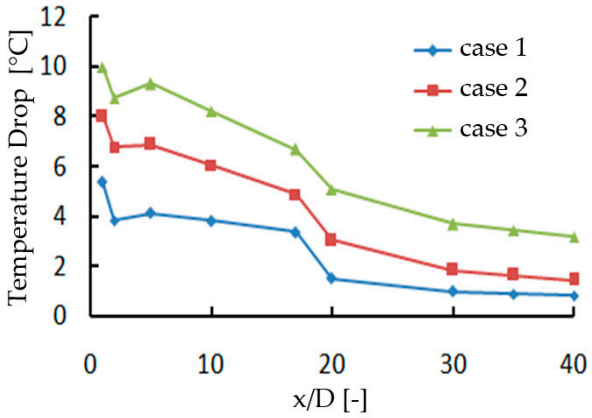

Figure14. Temperature decrease inside TBC along the centerline of the test plate top surface

Therefore, it is concluded that the heat insulation effect of TBC is grows more obvious when the radiation effect is significant. This is caused by the radiation property differences between TBC and nickel-based alloy. However, when TBC is coated, over 50% of the radiation heat transfer is reflected by TBC, which means TBC absorbs less radiation heat than superalloy and protects the metal substrate. Another advantage of TBC is that it smooths the temperature distribution and decreases the temperature gradient to some extent. More discussion can be found in [33].

5. Conclusion

Gas turbine film cooling system shows complicated flow and heat transfer characteristics due to the interaction of heat conduction, heat convection and radiation heat transfer. In the present study, the conjugate heat transfer characteristics of a film cooling system are experimentally and numerically analyzed. The topics include the radiation heat transfer, multi-composition gas and TBC. In solving the radiative heat transfer in the multi-composition field, the Discrete Transfer Model (DTM) and the Weighted Sum of Gray Gases (WSGG) spectral model are employed and validated.

The results show that the surface temperature increase significantly and the temperature gradient through the plate becomes much larger when the radiation is considered. It is also observed that a higher percentage of steam in gas composition results in a higher temperature (lower normalized temperature) on the film-cooled plate. In particular, the normalized temperature on the film-cooled plate decrease about 0.02 as the percentage of steam in hot gas increases per 7%.

Furthermore, the heat insulation effect of TBC grows more obvious when the radiation heat transfer is stronger. Also observed is that TBC smooths the temperature distribution and thus decreases the temperature gradient to some extent.

Nomenclature

a	Emission weighting factor	[-]
D	Diameter of the hole	[m]
I_{bv}	Spectral black body emission intensity	[$Wm^{-3}sr^{-1}$]
I_v	Spectral radiation intensity	[$Wm^{-3}sr^{-1}$]
I_{v0}	Radiation Intensity leaving the boundary	[$Wm^{-3}sr^{-1}$]
K_{av}	Spectral absorption coefficient	[m^{-1}]
K_{sv}	Spectral scattering coefficient	[m^{-1}]
k	Absorption coefficient	[m^{-1}]
L	Length of the hole	[m]
N_g	Number of gray gases	[-]
$\vec{r}$	Position vector	[m]
S	Radiation intensity source term	[$Wm^{-4}sr^{-1}$]
s	Path length	[m]
$\vec{s}$	Direction vector	[m]
T	Temperature	[K]
X, Y, Z	Cartesian coordinates	[m]
y^+	Dimensionless wall distance	[-]

Greeks

ε	Total gas emissivity	[-]
η	Normalized temperature	[-]
ν	Frequency	[s^{-1}]
Ω	Solid angle	[sr]

Subscripts

c	Coolant flow
g	Gas
j	Index
w	Wall

Acronyms

DTM	Discrete transfer model
RTE	Radiation transport equation
WSGG	Weighted sum of gray gases

Funding: This research was funded by Project 51076076 and 51110105013 supported by National Natural Science Foundation of China.

Acknowledgments: The authors appreciate the brilliant work of Dr. Wan, Wenping, Dr. Sun, Peng, Dr. Li, Mingfei and Dr. Yin, Hong on the thermally loaded film cooling test rig and the numerical simulation. Thanks also to Dr. Li, Weihong to summarize the work of the research group on the topic.

References

1. Mazzotta D W; Chyu M K; Alvin M A. Airfoil Heat Transfer Characteristics in Syngas and Hydrogen Turbines. *ASME Paper No. GT2007-28296*, 2007.
2. Bohn, D.; Bonhoff, C. Combined Aerodynamic and Thermal Analysis of a Turbine Nozzle Guide Vane. *IGTC Paper 95-108*, 1995
3. Bohn, D.; Heuer, T. Conjugate Flow and Heat Transfer Calculation of a High Pressure Turbine Nozzle Guide Vane. *AIAA 2001-3304*, 2001
4. Bohn, D.; Becker, V.; Kusterer, K.; Otsuki, Y.; Sugimoto, T. and Tanaka, R. 3-D Internal Conjugate Calculations of a Convectively Cooled Turbine Blade with Serpentine-Shaped Ribbed Channels. *IGTI Paper 99-GT-220*, 1999
5. Bohn, D.; Ren, J.; and Kusterer, K. Conjugate Heat Transfer Analysis for Film Cooling Configurations with Different Hole Geometry. *ASME IGTI Paper GT-2003-38369*, 2003.
6. Hansmann, T.; Wilhelmi, H.; and Bohn, D. An Experimental Investigation of the Film-Cooling Process at High Temperatures and Velocities. *AIAA-93-5062*, 1993.
7. Bohn, D.; Becker, V. 3-D Conjugate Flow and Heat Transfer Calculations of Film-Cooled Turbine Guide Vane at Different Operation Conditions. *ASME Paper 97-GT-23*, 1997.
8. Mansour, M.L.; Hosseini, K.M.; Liu, J.S. Assessment of the Impact of Laminar-Turbulent Transition on the Accuracy of Heat Transfer Coefficient Prediction in High Pressure Turbines. *ASME GT2006-90273*, 2006.
9. Heidmann, J.D.; Kassab, A.; Divo, E.A.; Rodriguez, F.; and Steinthorsson, E. Conjugate Heat Transfer Effects on a Realistic Film-Cooled Turbine Vane. *ASME IGTI Paper GT2003-38553*, 2003.
10. Hylton, L.D.; Milhec, M.S.; Turner, E.R.; Nealy, D.A.; and York, R.E. Analytical and Experimental Evaluation of the Heat Transfer Distribution Over the Surface of Turbine Vanes. *NASA CR 168015*,1983.
11. Hylton, L.D.; Nirmalan, V.; Sultanian, B.K.; and Kaufman, R.M. The Effects of Leading Edge and Downstream Film Cooling on Turbine Vane Heat Transfer. *NASA CR 182133*, 1988.
12. Dees, J. E.; Bogard, D. G.; Ledezma, G. A., et al. Overall and Adiabatic Effectiveness Values on a Scaled Up, Simulated Gas Turbine Vane: Part I---Experimental Measurements. *ASME Conference Proceedings*, 2011, 2011(54655): 571-582.
13. Ledezma, G. A.; Laskowski, G. M.; Dees, J. E.; et al. Overall and Adiabatic Effectiveness Values on a Scaled Up, Simulated Gas Turbine Vane: Part II---Numerical Simulations. *ASME Conference Proceedings*, 2011, 2011(54655): 595-605.
14. Dees, J. E.; Bogard, D. G.; Ledezma, G. A.; et al. The Effects of Conjugate Heat Transfer on the Thermal Field Above a Film Cooled Wall. *ASME Conference Proceedings*, 2011, 2011(54655): 607-617.
15. Kumar, A.; Kale, S.R. Numerical simulation of steady state heat transfer in a ceramic-coated gas turbine blade. *International Journal of Heat and Mass Transfer*, 2002, *45(24)*, pp. 4831-4845.
16. He, Zhi-hong; Tan, He-ping; Liu, Lin-hua; et al. Numerical computation on blade channel radiation in engine. *Journal of Propulsion Technology*, 2001, *22(01)*, pp. 65-68, 88.
17. Zhang, Li-fen; Liu, Zhen-xia; Lian, Xiao-chun. Numerical study of 3D heat transfer for turbine blade with air cooling. *Journal of Aerospace Power*, 2007, *22(08)*, pp. 1268-1272.
18. Akwaboa, S.; Mensah, P.; and Diwan, R. Effects of Thermal Radiation on Air Plasma Spray (APS) Coated Gas Turbine Blade. *ASME Paper No. GT2010-23660*, 2010.
19. Mazzotta, D.W.; Karaivanov, V.G.; Chyu, M.K.; and Slaughter, W.S. Gas-Side Heat Transfer in Syngas, Hydrogen-Fired and Oxy-Fuel Turbines. *ASME Paper GT2008-51474*, 2008.
20. Na, S.; Dennis, R.A.; Alsup, C.; Bryden, K.M., and Shih, T.I-P. Effects of Hot-Gas Composition on Temperature Distribution in a Flat Plate Cooled by Internal and Film Cooling. *ASME Paper GT2009-59727* , 2009.
21. Moliere, M.; and Belfort. Hydrogen-Fuelled Gas Turbines: Status and prospects. *2nd CAME-GT Conference*, Slovenia, 2004.
22. Feuerstein, A; Knapp, J; Taylor ,T; et al. Technical and economical aspects of current thermal barrier coating systems for gas turbine engines by thermal spray and EBPVD: A review. *Journal of Thermal Spray Technology*, 2008, *17(2)*: 199-213.
23. Bohn, D; and Krewinkel, R. Influence of a Broken-Away TBC on the Flow Structure and Wall Temperature of an Effusion Cooled Multi-Layer Plate Using the Conjugate Calculation Method. *ASME Conference Proceedings, 2008*, 2008(43147): p. 351-362.

24. Davidson, F.T.; Dees, J.E.; Bogard, D.G. An Experimental Study of Thermal Barrier Coatings and FilmCooling on an Internally Cooled Simulated Turbine Vane. *ASME Conference Proceedings*, 2011. *2011(54655)*: p. 559-570.
25. Cui, Y.F.; Xu, G.; Yu, B.; Nie, C.Q; and Huang, W.G. The Effects Of Pressure On Gas Turbine Combustor Performance: An Investigation Via Numerical Simulation. *ASME Paper No. GT2006-90635*, 2006.
26. Smith, T.F.; Shen, Z.F.; and Friedman, J.N. Evaluation of Coefficients for the Weighted Sum of Gray Gases Model. *Transactions of the ASME*, 1982, *104*, pp.602-608.
27. Krishnamoorthy, G. A New Weighted-Sumof-Gray-Gases Model for CO_2-H_2O Gas Mixtures. *International Communications in Heat and Mass Transfer*, 2010, *37*, pp.1182-1186.
28. Sun, P; Wang,W; Ren, J; Jiang, H. Effect of the Hot Gas Composition on a Highly Thermally Loaded Film Cooling System. *ASME Conference Proceedings*, 2011, *2011 (45593)*.
29. Kermanpur, A.; Varahram, N.; Davami, P.; and Rappaz, M. Thermal and Grain-Structure Simulation in a Land-Based Turbine Blade Directionally Solidified with the Liquid Metal Cooling Process. *Metallurgical and Materials Transactions B*, 2000, *31B(06)*, pp.1293-1304
30. Hottel, H.C.; Noble, J.J.; Sarofim, A.F.; Green, D.W.; Perry, R.H. Heat and Mass Transfer, *Chapter 5, in Perry's Chemical Engineers' Handbook*, 2007, *8th Edition*, McGraw-Hill, New York.
31. REFPROP, National Institute of Standards and Technology.
32. Wang, W.; Sun, P.; Ren, J. and Jiang, H. Radiative Effectiveness on the Aero- and Thermodynamics in a Highly Thermally Loaded Film Cooling System. *ASME Paper No. GT2011-45592*, 2011.
33. Li, M.; Yin, H.; Ren, J. and Jiang, H. Conjugate Heat Transfer Characteristics of a Highly Thermal-Loaded Film Cooling System in Hot and Multicomposition Gas Condition. J. Heat Transfer, 2015, 138(2), p.024503.